Cathodoluminescence and Photoconductive Characteristics of Single-Crystal Ternary CdS/CdSe/CdS Biaxial Nanobelts

*Linfeng Hu, Jian Yan, Yong Kim, Guangtao Fei, Kentaro Watanabe, Takashi Sekiguchi, Lide Zhang, and Xiaosheng Fang**

Rational design and synthesis of novel hybrid nanomaterials with precise control of morphology, structure and composition, has been an emerging topic in recent years.[1] These novel nanostructures generally enable intriguing electronic, optical or magnetic properties, and have yielded particular interests due to their potential applications on various nanodevices. For example, the photovoltaic device based on coaxial silicon nanowires consisting of a p-type silicon nanowire core capped with intrinsic and *n*-type silicon shells can serve as robust power sources to drive functional nanoelectronic sensors and logic gates.[2] High-quality Co_2Si–Al_2O_3 core-shell nanowires can be self-aligned as a gate electrode in a graphene transistor, which display ultra-high speed and scaled on-current.[3] In our previous study, we have developed some novel hybrid 1D nanomaterials including ZnS/ZnO biaxial nanobelts and ZnS/GaP core-shell nanocables.[4] Interestingly, such novel 1D nanomaterials exhibit superior optoelectronic properties such as high UV-light photosensitivity and tunable wavelength selectivity compared with the pure component.

Prof. L. F. Hu, Prof. X. S. Fang
Department of Materials Science
Fudan University
Shanghai 200433, P. R. China
E-mail: xshfang@fudan.edu.cn

Prof. J. Yan
School of Materials Science and Engineering
Hefei University of Technology
Hefei, Anhui 230009, P.R. China

Prof. Y. Kim
Department of Physics
Dong-A University
Hadan-2-dong, Sahagu, Busan 604-714, Korea

Prof. G. T. Fei, Prof. L. D. Zhang
Key Laboratory of Materials Physics and
Anhui Key Laboratory of Nanomaterials and Nanostructures
Institute of Solid State Physics
Hefei Institutes of Physical Science
Chinese Academy of Sciences, P. O. Box 1129
Hefei 230031, P. R. China

Dr. K. Watanabe, Prof. T. Sekiguchi
WPI Center for Materials Nanoarchitectonics
National Institute for Materials Science (NIMS)
Tsukuba, Ibaraki 305-0044, Japan

DOI: 10.1002/smll.201402545

CdS and CdSe are two important II-VI group compounds which have recently attracted considerable attention due to their primary band gaps of 2.42 and 1.74 eV respectively.[5] Functional devices based on CdS and CdSe nanostructures have been reported including nanolasers,[6] field effect transistors,[7] light-emitting diodes,[8] waveguides,[9] photodetectors etc.[10] More importantly, these semiconductors can form CdS/CdSe core-shell quantum dots through wet-chemical routes.[11] These hybrid quantum dots generally exhibit unique size- and structure-dependent properties, such as dramatic reduction in Auger recombination times,[12] ultrahigh photoluminescence quantum yield,[13] significantly improved electroluminescence external quantum efficiencies,[14] high energy conversion efficiency for dye-sensitized solar cells,[15] etc. Although quantum dots generally exhibit novel physical properties such as quantum confinement or surface effects, it is not easy task to construct various nanodevices based on an individual quantum dot and study the *in-situ* tunable properties of an individual CdS/CdSe unit. One-dimensional (1D) semiconducting nanomaterials are critical building blocks for nanodevice construction owing to their smooth surfaces, high surface-to-volume ratios and rationally designed surfaces. If 1D CdS/CdSe hybrid nanostructures could be synthesized, they would be very promising for optoelectronic devices due to their multiple functions originating from both CdS and CdSe. Inspired by this consideration, herein, we developed a novel hybrid nanostructure composed of single-crystal ternary CdS/CdSe/CdS biaxial nanobelt. Their unique cathodoluminescence (CL) and photoconductive properties have been clarified for the first time.

CdS/CdSe/CdS biaxial nanobelts were grown by a two-step physical vapor transport method as we have reported previously.[16] **Figure 1**a shows the typical scanning electron microscopy (SEM) image of the as-grown products, revealing high density of the resulting curved nanobelt-like structures with lengths of several tens of micrometers and diameter from several tens to several hundred nanometers. We applied transmission electron microscopy (TEM) and energy dispersive spectroscopy (EDS), and the corresponding results are shown in Figure 1b–e. A low magnification TEM image of a typical single nanobelt in Figure 1b reveals the clear interfaces between the side fragment and the central fragment. The elemental maps displayed in Figure 1c–e shed light on the distribution of the constituting Cd, S, and Se elements. One can

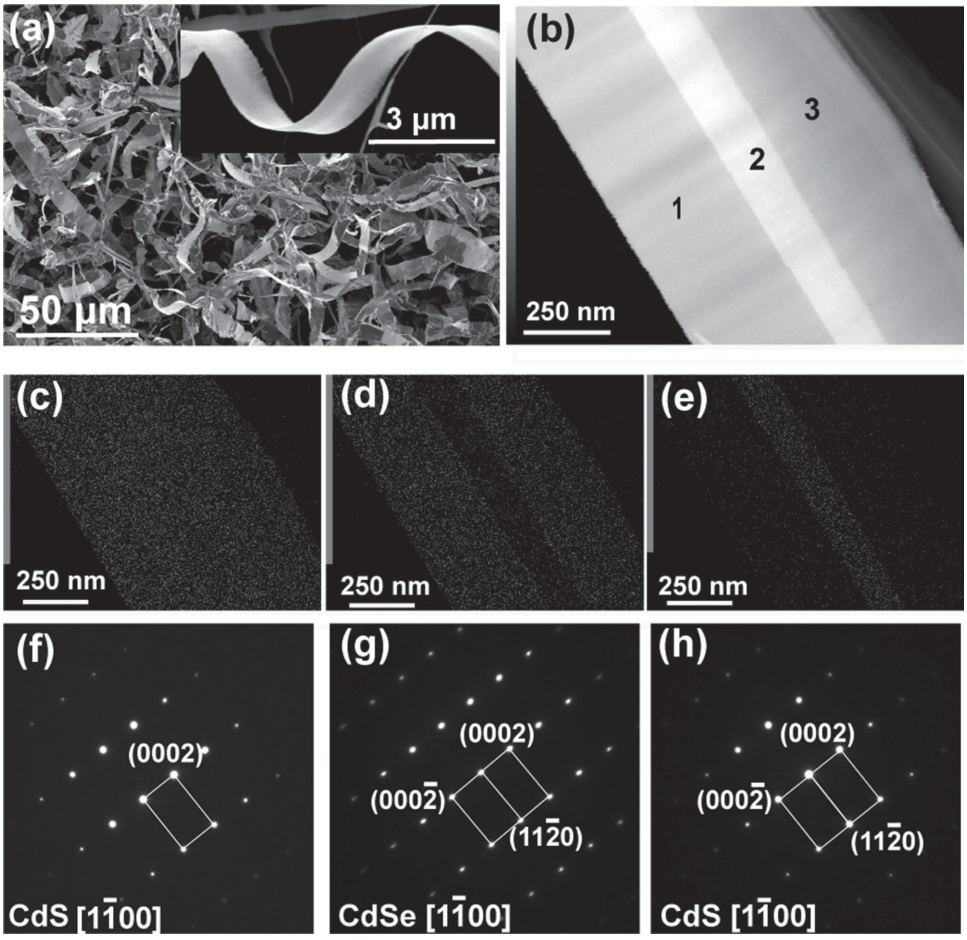

Figure 1. Typical (a) SEM and (b) TEM images of the as-grown CdS/CdSe/CdS biaxial nanobelts. EDS elemental mapping of (c) Cd, (d) S and (e) Se elements. (f–h) SAED patterns taken from three fragments taken from the areas labeled with 1, 2, and 3 in Figure 1b, respectively.

see that the Cd element uniformly covers the whole part of an individual nanobelt. However, S element mostly disturbs in the fringe side of the nanobelt, and the Se element spreads homogeneously in central part. These results clearly demonstrate a well-defined compositional profile of the CdS(side)/CdSe(centre)/CdS(side) triaxial nanobelt. Note that our previous study shows that central CdSe region shows sulfur contamination with a sulfur mole fraction ([S]/ [S] + [Se]) of ~0.3 confirmed by EDS analysis. However, such a EDS analysis gives a statistical result based on a large number of nanobelts rather than a single one due to the large diameter of incident electron beam. The side of CdS fragment is about 250 nm in width while the width of central CdSe part is about 100 nm. In order to obtain further structure information, the corresponding selected area electron diffraction (SAED) patterns of the central belt and the side layers taken from the area 1–3 labeled in Figure 1b are shown in Figure 1f–h, respectively. The SAED patterns with well-defined diffraction dots suggest the highly crystalline nature of the hybrid nanobelts. The three sets of SAED pattern exhibit similar patterns, which could be indexed to the wurtzite phase. Figure 1f and h are the SAED patterns taken from the side-part of the nanobelt, which could be well indexed to the wurtzite CdS phase. The SAED pattern taken from the central belt as shown in Figure 1g can be indexed to the wurtzite CdSe. The (0001) planes of the side CdS belt and the central CdSe belt are parallel to each other. This result reveals that the CdS/CdSe/CdS nanobelt grows along the $[11\bar{2}0]$ direction with ±(0001) planes as its side surfaces. Noting that the electron beam is parallel to $[1\bar{1}00]$ direction, these results confirm that the as-synthesized nanobelts are of a structure of side-to-side triaxial nanobelts.

The highly crystalline nature of the CdS/CdSe/CdS nanobelt was further verified by high-resolution transmission electron microscopy (HRTEM) characterization in **Figure 2**. The HRTEM images of the side CdS belt ribbon, the central CdSe layer, and the interface area, are shown in Figure 2b–d, respectively. All of them exhibit clear lattice fringes, which reveal that both the high crystallinity nature of both inner ribbon and the side layer. Figure 2b and d are taken from the two side CdS fragments of an individual CdS/CdSe/CdS nanobelt. The *d*-spacings indicated by parallel lines are 0.335 nm and 0.207 nm closely correspond to the distance between the (0002) planes and $(11\bar{2}0)$ planes of wurtzite CdS, respectively. Figure 2c shows the HRTEM image taken from the central part of the hybrid nanobelt, in which the 0.35 nm spacing of the lattice fringes agrees well with the expected separation of CdSe (0002) planes. Then more attention has been paid to the interfacial area between the CdS fragment and CdSe part. As shown in Figure 2d, it is hard to distinguish the exact CdS/CdSe interface as the contrast in not obvious,

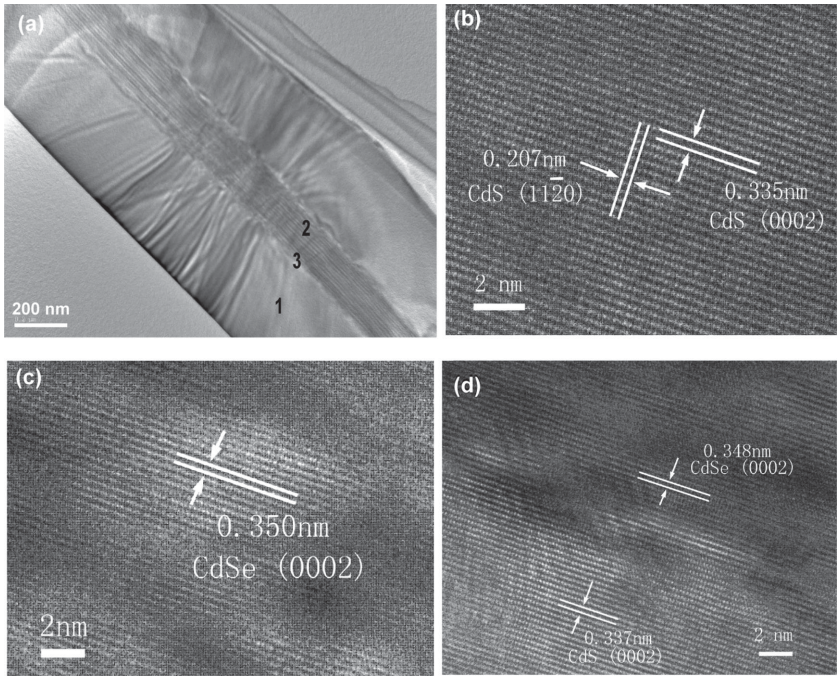

Figure 2. (a) A low magnification TEM image of single CdS/CdSe/CdS nanobelt. (b–d) the HRTEM images taken from the areas labeled with domain 1, 2, 3 in (a), respectively.

although the contrast is very clear in low magnification TEM images in Figure 1b and 2a. A little low lattice mismatch (<4%) of (11$\bar{2}$0) CdS/(11$\bar{2}$0) CdSe might be responsible for this result. The *d*-spacings indicated by lines are 0.337 nm and 0.348 nm corresponding to the distance between the (0002) planes of wurtzite CdS and CdSe, respectively. It is worth to note that the *d*-spacing of (0002) planes of wurtzite CdS at the interface (0.337 nm) is little larger than that (0.335 nm) in the side CdS fragment. Meanwhile, the *d*-spacing of (0002) planes of wurtzite CdSe at the interface (0.348 nm) is slightly smaller than that in the central CdSe fragment (0.350 nm). Such a change in *d*-spacing is possibly attributed to the lattice relaxation at the CdS/CdSe heterostructured interface. Recently, Wang *et al.* have demonstrated that the ±(0001) planes of wurtzite structure exhibit polarity, favoring the secondary growth of nanowires,[17] Zhang *et al.* also reported the epitaxial growth of SnO_2 on the side faces of ZnO nanobelts.[18] Note that the CdS and CdSe both possess wurtzite structure, and the lattice parameters between these two phases are fairly close to each others, allowing the epitaxial growth of CdS on the side of CdSe nanobelts. In the present study, the CdS/CdSe/CdS hybrid nanobelts are formed by a two-step physical vapor transport method, and the CdS ± (0001) side surfaces are epitaxially grown along the ± (0001) plane of CdSe species.[16]

Cathodoluminescence (CL) is an important property for semiconductor nanostructures caused from the emission of light as a result of electron bombardment. As compared to other techniques, such as photoluminescence (PL) spectroscopy, CL has the advantage of higher spatial resolution, down to few tens of nanometers. In the present study, the optical properties of individual CdS/CdSe/CdS nanobelt dispersed on standard C-coated TEM copper grids were studied using the similar method as our previous work (**Figure 3**a). In order to further study the spatial variation of optical properties, CL spectra at different spots along different part on an individual nanobelt are recorded at room temperature as shown in Figure 3b. One can see that the CL spectrum as shown in Figure 3b mainly consists of two sharps emission peaks at 710 nm, 515 nm, respectively. Since CdS and CdSe shows a direct band gap of 2.42 and 1.73 eV, respectively, the as-observed emission at 515 nm and 710 nm should be respectively originated from the outer CdS layer and inner CdSe layer. No evidence of the transient region between CdS and CdSe layer has been found in our study. Furthermore, the side part (spot 1 and 3) generally displays CdS CL emission at 515 nm (2.41 eV), which gradually disappears along the axis direction. The appearance of 1.73 eV emission from CdSe phase with a very low intensity in spot 1 might be attributed to the image shift under the TEM observation due to the very small area of the outside CdS shell. The spot 2 located in the central part of the nanobelt mainly shows the CL emission from the CdSe phase. Such a result agrees well with the composition distribution as obtained from the aforementioned SEM and TEM observations. Figure 3c and d depict the corresponding CL images of the nanobelt recorded at 2.41 eV and 1.75 eV, respectively. Well-monochromated CL image with uniform distribution is apparent in these images, and the emission intensity of these images is well consistent with the result in Figure 3b.

The well-defined 1D morphology of the CdS/CdSe/CdS nanobelt with high surface-area ratio and smooth top surface affords facility for the device construction based on an individual nanobelt. Then, we turn to the in-situ photoresponsive behavior of a CdS/CdSe/CdS biaxial nanobelt unit. As illustrated in **Figure 4**a, a pair of 2.5-μm spaced Cr/Au electrodes

www.MaterialsViews.com

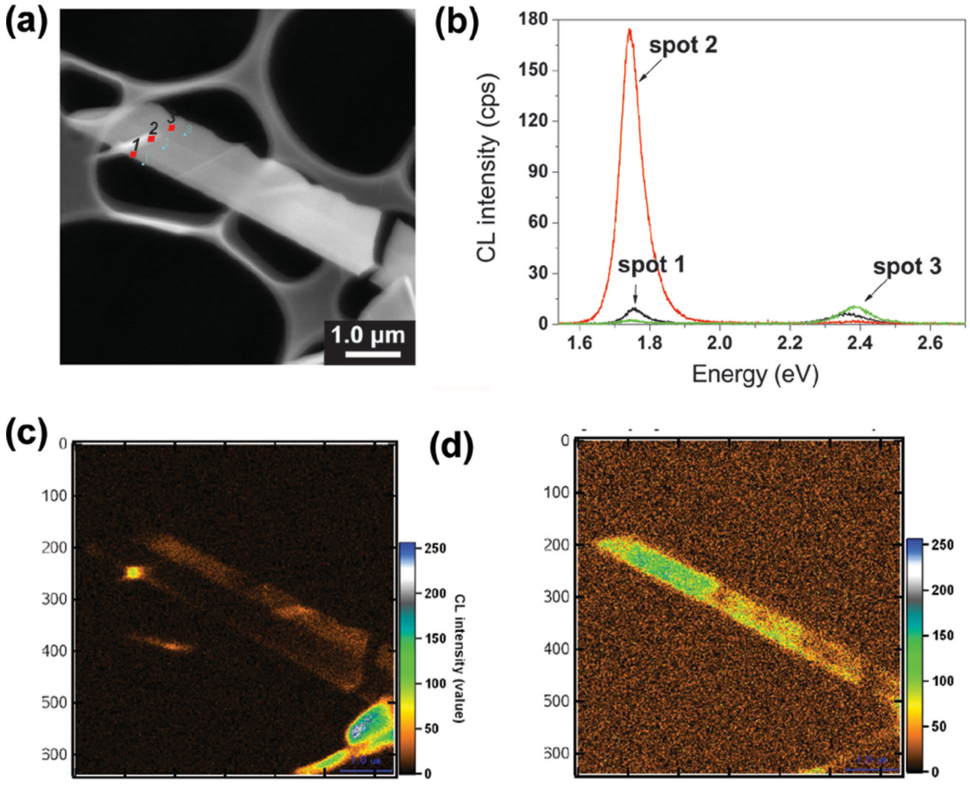

Figure 3. (a) Typical SEM image of a CdS/CdSe/CdS nanobelt and (b) CL spectra from the three distinctive spots in (a). CL image of the same nanobelt recorded at (c) 515 nm (2.41 eV), (d) 710 nm (1.75 eV), respectively.

(10 nm/100 nm) was deposited on a CdS/CdSe/CdS biaxial nanobelt with a diameter of ~1.2-μm dispersed at a SiO_2/Si substrate by standard lithography procedures to form a top-contacted device. *I–V* measurements were performed on this device by a two-probe method under ambient air conditions. As shown in Figure 4b, the dark current of the present device is very low photocurrent of 0.07 pA at an applied voltage of 5.0 V. Under illumination of a 600 nm light, the device

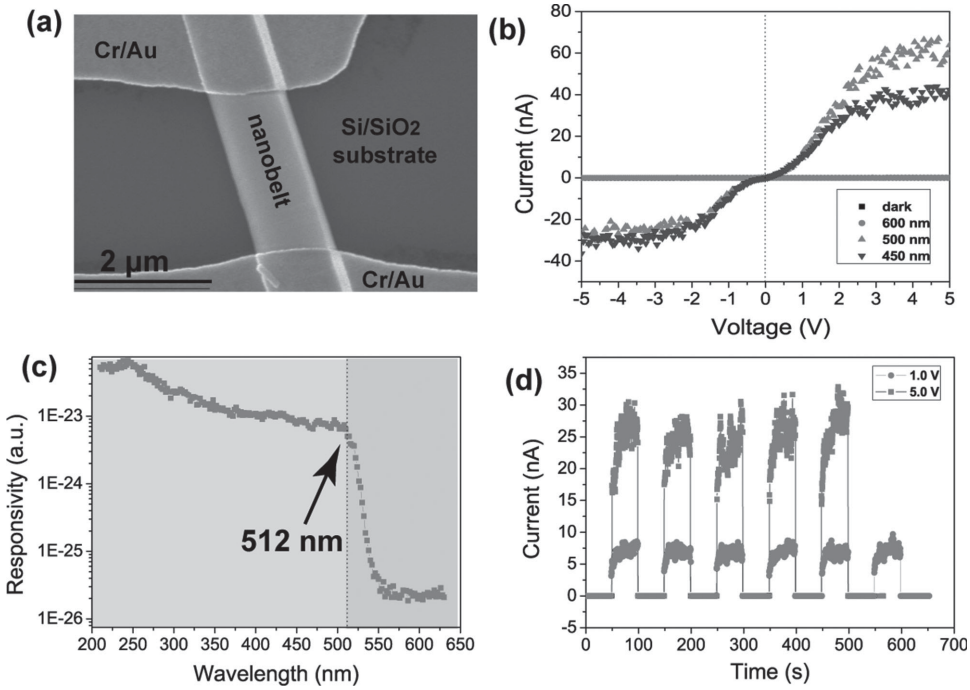

Figure 4. (a) A typical SEM image of a photodetector constructing from an individual CdS/CdSe/CdS nanobelt. (b) Current-voltage (*I–V*) characteristics of the CdS/CdSe/CdS nanobelt photodetector illuminated with 450–600 nm light and under dark conditions. (c) Spectral photoresponse measured from the UV-light device at a bias of 10.0 V. (d) The reproducible on/off switching upon 450 nm light illumination at a bias of 1.0 and 5.0 V, respectively.

Table 1. An Overview of dark current, photocurrent, photo-current on/off ratio, R_λ and external quantum efficiency (*EQE*) of the photodetectors constructed from pure CdS, CdSe nanostructure and biaxial CdS/CdSe/CdS nanobelt.

Photodetectors	Dark Current	Photocurrent	Photo-current on/off ratio	R_λ (A/W)	*EQE* (%)	Reference
pure CdSe nanowie	25 pA (at 2.0 V)	5.0 nA (at 2.0 V)	200	1.7 ± 0.3	—	[19a]
pure CdS nanobelt	~5 μA (at 1.0 V)	~30 μA (at 1.0 V)	6	73000	1.9 × 107	[20]
biaxial CdS/CdSe/CdS nanobelt	0.07 pA (at 5.0 V)	63.8 nA (at 5.0 V)	911	642	2.56 × 105	This work

exhibits no apparent increase compared with that obtained in the dark. However, it drastically increases to 63.8 nA under 500 nm-light illumination (2.81 mW cm^{-2}) at an applied voltage of 5.0 V due to the electron-hole pairs excited by the incident photons with energy larger than the band gap. Note that the ON/OFF current ratio of this increase is as high as 911, which is much higher than that of some pure CdS or CdSe nanobelt in the previous reports (**Table 1**). In general, R_λ and EQE are two critical parameters to determine the sensitivity for an optoelectronic device, which can be expressed by: $R_\lambda = \frac{\Delta I}{PS}$ and $EQE = \frac{hc}{e\lambda}\cdot\frac{\Delta I}{PS}$, respectively. [14] Wherein, ΔI is the difference between photo-excited current and dark current, P is the light power density irradiated on the nanobelt, and S is the irradiated area of an individual nanobelt, λ is the exciting wavelength, h is Planck's constant, c is the velocity of the light, and e is the electronic charge. The calculated R_λ and EQE values of the present CdS/CdSe/CdS biaxial nanobelt are as high as 6.4×10^2 A/W and 2.56×10^5% irradiated by 500 nm light at an applied voltage of 5.0 V, respectively. Such a result indicates a high sensitivity of the present device. Figure 4c displays the spectral photoresponse of the device at a bias of 5.0 V at different wavelengths from 210 to 630 nm. The sensitivity is relatively low when the wavelength is higher than 512 nm, and apparently increases by about three orders of magnitude when the device is illuminated by a light with energy above this threshold wavelength. Such a result is obviously different from that obtained from a pure CdSe nanobelt,[19] but similar with the one detected from an individual CdS nanobelt,[20] suggesting the CdS phase in the ternary hybrid nanobelts plays a key role in the photoresponsive behavior. This result is quite different with that reported in our previous work for ZnS/ZnO biaxial nanobelts.[4a] The real reason is still unclear, and we propose that this phenomenon might be attributed to the charge injection from CdSe to CdS and then recombination by band-bending at CdS and CdSe junction. Recently, Y. Lee et al. have confirmed that the insertion of a CdS layer between TiO_2 and CdSe can elevate the conduction band edge of CdSe in a TiO_2/CdS/CdSe ternary system.[21] This change in band structure gives a higher driving force for the injection of excited electrons out of CdSe layer. Analogously, the injection of excited electrons from the CdSe central part to the CdS side might be possible in our CdS/CdSe/CdS nanobelt, leading to the similar spectral photoresponse as that of pure CdS nanobelt. Some investigation is still underway to further reveal the photoconductive mechanism of the present CdS/CdSe/CdS nanobelts. Repeatability and response speed are key parameters which determine the ability of a photodetector under a quickly varying optical signal. Figure 4d shows the time response of the CdS/CdSe/CdS nanobelt-based device. No abrupt degradation of photoresponsive behavior was detected after several tens of on/off switching cycles, confirming the excellent cycle stability and high response speed of the present device.

In summary, we have successfully grown CdS/CdSe/CdS biaxial nanobelt with well-defined morphology by a facile chemical vapor deposition route. The cathodoluminescence and optoelectronic properties based on an individual CdS/CdSe/CdS biaxial nanobelt were firstly revealed. Both typical CdS and CdSe emissions have been detected from the as-grown CdS/CdSe/CdS nanobelts. The photodetector based on this novel nanobelt exhibits high sensitivity and excellent cycle stability. Such a CdS/CdSe/CdS biaxial nanobelt might be very promising for potential applications due to its novel hybrid structure, large surface-to-volume ratio and distinct optoelectronic properties. The present study opens a new door to rationally design of hybrid cadmium chalcogenide compounds and to develop their corresponding novel physical properties.

Experimental Section

CdS/CdSe/CdS biaxial nanobelts were synthesized by a thermal evaporation method as we reported previously.[16] The morphology of the nanobelts was characterized by a field-emission SEM (JSM-6700F), and a TEM (JEM-3000F) coupled with X-ray energy dispersive spectrometry (EDS). Spatially resolved CL spectra from individual structures were collected with a high-resolution CL system at an accelerating voltage of 5 kV and a current of 480 pA at room temperature using a Schottky SEM (S-4300SE/N, Hitachi Hightechnologies) equipped with a CL system (Horiba). An individual CdS/CdSe/CdS biaxial nanobelt was assembled as a nanoscaled photodetector by standard lithography procedures similar to the method in our previous study.[19] The current-voltage (*I–V*) characteristics of the individual nanobelt photodetector were measured using an Advantest Picoammeter R8340A and a dc voltage source R6411. A spectral response for different wavelengths was recorded by using a xenon lamp (500 W).

Acknowledgements

LFH and JY contributed equally to this work. This work was supported by the National Basic Research Program of China (Grant No. 2012CB932303), the National Natural Science Foundation of China (Grant Nos. 51471051 and 51372040), Shanghai Pujiang Program (12PJ1400300), Innovation Program of Shanghai Municipal

Education Commission (14ZZ003), Shanghai Shu Guang Project (12SG01), Science and Technology Commission of Shanghai Municipality (13NM1400300), the Programs for Professor of Special Appointment (Eastern Scholar) at Shanghai Institutions of Higher Learning and for New Century Excellent Talents in University (NCET-11–0102). The part of work by YK was partially supported by the Basic Science Research Program through the National Research Foundation of Korea (NRF) funded by the Ministry of Education, Science and Technology (2012R1A1A2002076).

[1] P. D. Yang, *MRS Bull.* **2012**, *37*, 806.
[2] B. Z. Tian, X. L. Zheng, T. J. Kempa, Y. Fang, N. F. Yu, G. H. Yu, J. L. Huang, C. M. Lieber, *Nature* **2007**, *449*, 885.
[3] L. Liao, Y. C. Lin, M. Q. Bao, R. Cheng, J. W. Bai, Y. Liu, Y. Q. Qu, K. L. Wang, Y. Huang, X. F. Duan, *Nature* **2010**, *467*, 305.
[4] a) L. F. Hu, M. Y. Liao, H. J. Xiang, X. G. Gong, L. D. Zhang, X. S. Fang, *Adv. Mater.* **2012**, *24*, 2305; b) L. F. Hu, M. M. Brewster, X. J. Xu, C. C. Tang, S. Grade ak, X. S. Fang, *Nano Lett.* **2013**, *13*, 1941.
[5] C. M. Lieber, Z. L. Wang, *MRS Bull.* **2007**, *32*, 99.
[6] X. F. Duan, Y. Huang, R. Agarwal, C. M. Lieber, *Nature* **2003**, *421*, 241.
[7] R. M. Ma, L. Dai, G. G. Qin, *Nano Lett.* **2007**, *7*, 868.
[8] S. C. Erwin, L. J. Zu, M. Haftel, A. L. Efros, T. A. Kennedy, D. J. Norris, *Nature* **2005**, *436*, 91.
[9] A. B. Greytak, C. J. Barrelet, Y. Li, C. M. Lieber, *Appl. Phys. Lett.* **2005**, *87*, 151103.
[10] J. S. Jie, W. J. Zhang, Y. Jiang, X. M. Meng, Y. Q. Li, S. T. Lee, *Nano Lett.* **2006**, *6*, 1887.
[11] X. G. Peng, M. C. Schlamp, A. V. Kadavanich, A. P. Alivisatos, *J. Am. Chem. Soc.* **1997**, *119*, 7019.
[12] F. García-Santamaría, S. Brovelli, R. Viswanatha, J. A. Hollingsworth, H. Htoon, S. A. Grooker, V. I. Klimov, *Nano Lett.* **2011**, *11*, 687.
[13] W. N. Nan, Y. Niu, H. Y. Qin, F. Cui, Y. Yang, R. C. Lai, W. Z. Lin, X. G. Peng, *J. Am. Chem. Soc.* **2012**, *134*, 19685.
[14] B. N. Pal, Y. Ghosh, S. Brovelli, R. Laocharoensuk, V. I. Klimov, J. A. Hollingsworth, H. Htoon, *Nano Lett.* **2012**, *12*, 331.
[15] Y. L. Lee, Y. S. Lo, *Adv. Funct. Mater.* **2009**, *19*, 604.
[16] Y. L. Kim, J. H. Jung, H. S. Yoon, M. S. Song, S. H. Bae, Y. Kim, Z. G. Chen, J. Zou, H. J. Joyce, Q. Gao, H. H. Tan, C. Jagadish, *Nanotechnology* **2010**, *21*, 145602.
[17] a) Z. L. Wang, X. Y. Kong, J. M. Zuo, *Phys. Rev. Lett.* **2003**, *91*, 185502, b) C. Ma, Z. L. Wang, *Adv. Mater.* **2005**, *17*, 2635; c) D. Moore, C. Ronning, C. Ma, Z. L. Wang, *Chem. Phys. Lett.* **2004**, *385*, 8.
[18] J. W. Zhao, C. H. Ye, X. S. Fang, L. R. Qin, L. D. Zhang, *Crystal Growth & Design* **2006**, *6*, 2643.
[19] a) S.-C. Kung, W. D. Xing, W. E. Veer, F. Yang, K. C. Donavan, M. Cheng, J. C. Hemminger, R. M. Penner, *ACS Nano* **2011**, *5*, 7627; b) Y. Jiang, W. J. Zhang, J. S. Jie, X. M. Meng, X. Fan, S.-T. Lee, *Adv. Funct. Mater.* **2007**, *17*, 1795.
[20] L. Li, P. C. Wu, X. S. Fang, T. Y. Zhai, L. Dai, M. Y. Liao, Y. Koide, H. Q. Wang, Y. Bando, D. Golberg, *Adv. Mater.* **2010**, *22*, 3161.
[21] a) Y.-L. Lee, Y.-S. Lo. *Adv. Funct. Mater.* **2009**, *19*, 604; b) Y.-L. Lee, C.-F. Chi, S.-Y. Liau, *Chem. Mater.* **2010**, *22*, 922; c) L.-W. Chong, H.-T. Chien, Y.-L. Lee, *J. Power Sources* **2010**, *195*, 5109.

Received: August 24, 2014
Published online: November 10, 2014